

Interplay of metallicity, ferroelectricity and layer charges in $\text{SmNiO}_3/\text{BaTiO}_3$ superlattices

Edith Simmen* and Nicola A. Spaldin
Materials Theory, ETH Zurich, Switzerland
(Dated: September 27, 2024)

Using density-functional theory, we demonstrate that the formal layer charges of the metallic samarium nickelate electrode influence the spontaneous ferroelectric polarization of the barium titanate in $\text{SmNiO}_3/\text{BaTiO}_3$ capacitors. We find that, despite the metallic screening of SmNiO_3 , the spontaneous polarization of BaTiO_3 always aligns with the layer polarization of the SmNiO_3 formal charges. We also find zero critical thickness for the ferroelectricity in BaTiO_3 in this orientation. The opposite polarization direction is highly disfavored for thin BaTiO_3 slabs but becomes less unstable with increasing slab thickness. We construct a simple electrostatic model that allows us both to study the behavior for thicker BaTiO_3 and SmNiO_3 slabs and to extract the influence of various material parameters on the behavior. We mimic a metal-insulator transition in the SmNiO_3 by varying the metallic screening length, which we find greatly influences the stability of the ferroelectric polarization. Our results show that the layer charges in the metal electrodes strongly influence the properties in ferroelectric capacitors and in fact can provide new ways to control the ferroelectric properties.

I. INTRODUCTION

Thin-film ferroelectrics are a subject of active research interest both because of their fundamental interest and for their potential applications in low-energy electronic technologies [1–4], such as ferroelectric tunnel junctions [1, 3] or ferroelectric field-effect devices[3]. For most of these applications, the ferroelectric films are grown in a capacitor geometry with metallic electrodes. The electrode is needed to control or read out the ferroelectric state [2] and to screen interface charges that accumulate due to the spontaneous polarization $\mathbf{P}_{\text{spont}}$ of the ferroelectric film. In the absence of such screening, these interface charges lead to a depolarizing field that counteracts and suppresses the polarization [5].

While perovskite oxide metals provide good coherence with perovskite ferroelectrics, they can contain formally positively or negatively charged ions. For example, the formally +3 charges of the A- and B-site cations in the rare-earth nickelates RNiO_3 lead to a metallic phase with charged (001) RO^+ and NiO_2^- layers. In their insulating states, the layer charges would lead to a polar discontinuity at the interface to a material with no or different layer charges [6]. Such a polar discontinuity has been studied in detail in the ferroelectric III-III perovskite BiFeO_3 , either at the surface [7] or at the interface to the II-IV SrRuO_3 electrode [8, 9]. The resulting polar discontinuity strongly favors one of the two polarization directions [8]. The polarization direction minimizing the interface charges, referred to as the ‘happy’ polarization [7] is much lower in energy than the opposite, ‘unhappy’ polarization which increases the interface charges. In the metallic state of the rare-earth nickelates, the additional metallic screening could reduce or erase the effects of this polar discontinuity.

The interface charge σ_{inter} resulting from the polar discontinuity between a III-III and II-IV perovskite is determined by the bulk polarizations $\mathbf{P}_{\text{bulk},i}$ of the two materials i forming the interface [6].

$$\sigma_{\text{inter}} = (\mathbf{P}_{\text{bulk},1} - \mathbf{P}_{\text{bulk},2}) \cdot \hat{n} \quad (1)$$

In addition to the spontaneous polarization, the layer polarization $\mathbf{P}_{\text{layer}}$ also contributes to the bulk polarization, described by $\mathbf{P}_{\text{bulk},i} = \mathbf{P}_{\text{spont}} + \mathbf{P}_{\text{layer}}$. Here, the polarization vector of $\mathbf{P}_{\text{layer}}$ is formed by the charged layers in the III-III perovskite. The layer polarizations can be calculated from the formal charges Z_i and positions r_i of all atoms i in the unit cell of volume Ω using $\frac{e}{\Omega} \sum_i r_i \cdot Z_i$.

Fig. 1a illustrates the interface between a representative III-III (SmNiO_3) and a II-IV (BaTiO_3) perovskite material. For centrosymmetric SmNiO_3 ($P_{\text{spont}} = 0$), the layer polarization in Fig. 1 is $50 \mu\text{C cm}^{-2}$ (upper arrow). Considering the opposite surface normals, the NiO_2^- and SmO^+ surface have a respective charge of $-50 \mu\text{C cm}^{-2}$ and $+50 \mu\text{C cm}^{-2}$ [6]. Assuming cubic symmetry in the BaTiO_3 , both spontaneous polarization (P_{BTO}) and layer polarization are zero, giving zero bulk polarization. When subtracting the bulk polarization of BaTiO_3 from SmNiO_3 , we find $\sigma_{\text{inter}} = -50 \mu\text{C cm}^{-2}$ and $+50 \mu\text{C cm}^{-2}$ for the upper NiO_2/BaO and lower SmO/TiO_2 interfaces, respectively.

If the spontaneous polarization in either material is non-zero, the interface charge will change accordingly. The polar discontinuity can be partially compensated if the spontaneous polarization in the BaTiO_3 aligns with the layer polarization (middle arrow in Fig. 1b) and/or if a spontaneous polarization forms inside the SmNiO_3 opposite to the layer polarization (bottom arrow). Interface charges increase when the polarization directions in either material are inverted. For a detailed discussion of the interface charges between III-III and II-IV perovskites, see reference [8].

In this study, we examine the effect of screening

* edith.simmen@mat.ethz.ch

charges from metal electrodes on the polar discontinuity between SmNiO_3 and BaTiO_3 . The effect of layer polarization within metal electrodes on ferroelectric capacitors has been touched on in the literature, for the cases of LaNiO_3 [10–12] and $\text{La}_{1-x}\text{Sr}_x\text{MnO}_3$ (LSMO) [9]. In Ref.[10], a preferred polarization direction for BaTiO_3 was identified in DFT calculations of asymmetric $\text{LaNiO}_3/\text{BaTiO}_3/\text{LaNiO}_3$ heterostructures due to the polar discontinuity. In symmetric $\text{LaNiO}_3/\text{BaTiO}_3$ superlattices, Ref. [11] reported improved screening of the polar discontinuity at the $\text{NiO}_2^-/\text{BaO}$ interface in DFT, leading to stronger ferroelectricity at low thicknesses. While internal field due to polar discontinuity was estimated to be negligibly small compared to the experimental coercive voltages in $\text{LaNiO}_3/\text{PZT}$ heterostructures [12], Ref. [9] measured a shift in the hysteresis loop of PZT-LSMO heterostructures consistent with the polar discontinuity.

Motivated by these considerations, we perform a detailed study of the role of layer charges at the ferroelectric-metallic interface in ferroelectric BaTiO_3 capacitors with formally charged layers in the metallic SmNiO_3 electrodes. BaTiO_3 is a prototypical ferroelectric with a polar, tetragonal phase at room temperature [13]. Metallic SmNiO_3 is orthorhombic with $Pbnm$ symmetry [14] and has NiO_6 octahedral rotations corresponding to the Glazer notation $a^-a^-c^+$. Like all members of the rare-earth nickelate family (except for LaNiO_3), SmNiO_3 has a high-temperature metallic phase and undergoes a sharp transition to an insulating phase upon cooling. Importantly for practical applications, the metal-insulator transition (MIT) in SmNiO_3 is just above room temperature (400 K [15]), allowing for easier control of the MIT in the lab.

We start by investigating the effect of the formal polar discontinuity on the spontaneous polarization in BaTiO_3 using density-functional theory (DFT). We confirm that the polarization in superlattices with charged layers within the metallic electrode shows a clear preference for the happy orientation and is not switchable for thin slabs. In addition, we find the absence of a critical thickness in BaTiO_3 for the polarization orientation minimizing the interface charges. Using an electrostatic model, we study the polar discontinuity in thicker slabs and examine the effects of the dielectric permittivity and the metallic screening length on the system. As the slab thickness increases, the unhappy orientation becomes less unstable. We find that the effect of the polar discontinuity on the ferroelectric is reduced for a smaller effective metallic screening length and a higher dielectric constant. Lastly, we discuss the physical meaning of the parameters in the electrostatic models and different ways to retrieve them from DFT.

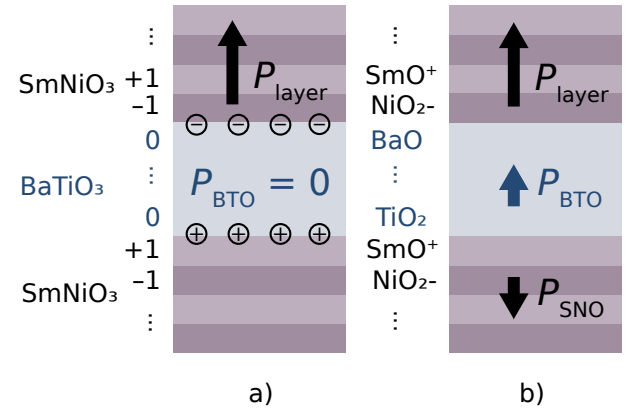


Figure 1: Illustration of the polar discontinuity resulting from the formal layer charges in $\text{SmNiO}_3/\text{BaTiO}_3$ superlattices. a) Paraelectric BaTiO_3 . The charged layers of ± 1 electron charge per formula unit lead to a layer polarization P_{layer} in SmNiO_3 and to a net positive or negative charge at the interface to the II-IV perovskite BaTiO_3 . b) Ferroelectric BaTiO_3 . The interface charges are partially compensated when the spontaneous polarization P_{BTO} in BaTiO_3 aligns with and the polar displacements P_{SNO} of SmNiO_3 are opposite to P_{layer} .

II. METHODS

We calculated the properties of superlattices of BaTiO_3 and SmNiO_3 using density-functional theory (DFT) as implemented in the VASP Code [16, 17]. We describe the exchange-correlation with the Perdew-Burke-Ernzerhof functional revised for solids (PBEsol) [18]. Projector augmented-wave (PAW) pseudopotentials [19, 20] were used with the following valence electrons (name of VASP pseudopotential): $5s^25p^66s^2$ (Ba_{sv}), $3p^64s^23d^4$ (Ti_{sv}), $2s^22p^4$ (O), $3p^64s^23d^8$ (Ni_{pv}) and $5s^25p^66s^25d^1$ (Sm_{3}), with the f electrons of Sm frozen into the core. In-plane, the superlattices were constructed from supercells of 1×1 formula units when the rotations in SmNiO_3 were disabled (Fig. 2b) and from supercells of $\sqrt{2} \times \sqrt{2}$ formula units when they were allowed (Fig. 3b). Out-of-plane, the superlattices were constructed from layers of 5 BaTiO_3 and 4 SmNiO_3 formula units unless stated otherwise. The in-plane lattice parameters were constrained to the calculated cubic SrTiO_3 lattice parameters of $a = 3.898 \text{ \AA}$ from Ref. [21] and the c -axis vector was allowed to relax to its lowest energy value. We used an energy cut-off of 650 eV and the structure was relaxed until the forces on the atoms were less than 0.01 eV \AA^{-1} . We employed $8 \times 8 \times 1$ and $16 \times 16 \times 1$ Monkhorst-Pack k-point grids [22] during relaxations for superlattices with active and disabled rotations in SmNiO_3 respectively, and for density-of-states (DOS) calculations, the k-point grid was doubled in-plane.

The relaxations of the ‘happy’ superlattices were performed in two steps: first, we relaxed only SmNiO_3 while fixing BaTiO_3 to its high-symmetry cubic reference structure, and next, we relaxed all atoms in the superlattice. For the ‘unhappy’ relaxations, 1-3 layers of BaTiO_3 were fixed to the bulk oppositely polarized structure.

We evaluated the local spontaneous polarization resolved by layers by summing the products of the formal charges Z and the displacement \mathbf{d} from their centrosymmetric position along the c axis over all ions i in the layer according to

$$\mathbf{P}_{\text{loc}} = \frac{e}{\Omega} \sum_i \Delta \mathbf{d}_i \cdot Z_i, \quad (2)$$

with e and Ω being the elementary charge and the volume of the corresponding layer, respectively. The height of one layer corresponds to the distance from one A atom (A = Ba, Sm) to the next, equivalent to the height of one formula unit along the c -axis. The analogous summation in bulk BaTiO_3 with the in-plane lattice parameters set to those of SrTiO_3 yields a polarization of $P_{\text{BaTiO}_3} = 28.6 \mu\text{C cm}^{-2}$. To quantify polar displacements in metallic SmNiO_3 , we also calculated the ionic off-centering using Eq. 2, recognizing that the resulting quantity is not a true polarization because of the metallicity.

Phonon frequencies at the Γ point were calculated on 5 atom BaTiO_3 and 20 atom SmNiO_3 unit cells using the atomate2 [23] phonon workflow, and any post-processing was done using phonopy [24, 25].

III. RESULTS

A. Properties of superlattices with SmNiO_3 rotations disabled

We start by investigating simplified superlattices with the octahedral rotations of SmNiO_3 disabled. Our motivation for studying this simplified structure is twofold: First, fewer in-plane unit cells are needed thus reducing the computational time. Second, previous studies on similar superlattices with LaNiO_3 and BaTiO_3 [26] or PbTiO_3 [12, 27] have focused on superlattices with disabled octahedral rotations. By doing the same, we can both compare our results to literature and validate this approximation.

We begin by calculating the layer-resolved DOS of $(\text{BaTiO}_3)_5(\text{SmNiO}_3)_4$ with both BaTiO_3 and SmNiO_3 constrained to the high-symmetry cubic perovskite structure. Fig. 2a shows the results in green with SmO/TiO_2 as the lower and NiO_2/BaO as the upper interface in the superlattice. We note a clear shift of the BaTiO_3 bands to higher energies (black triangles) when going from the lowest to the highest BaTiO_3 layer which indicates the presence of an electric field inside the BaTiO_3 layer. We can assign the origin of this electric field to the polar discontinuity and the resulting charges at the interface

between SmNiO_3 and BaTiO_3 . We conclude that, despite being metallic, SmNiO_3 cannot fully screen these interface charges.

Next, we relax the structure. We find that, as expected, the BaTiO_3 slab develops a spontaneous polarization. The corresponding displacements of Ti with respect to O atoms are visible in Fig. 2b, and in Fig. 2c we show the resulting local polarization calculated using Eq. 2. First, we relax only the BaTiO_3 slab and BaTiO_3 develops a polarization of $30 \mu\text{C cm}^{-2}$ (blue line in Fig. 2) very close to its bulk value of $29 \mu\text{C cm}^{-2}$ (gray line). The polarization in the BaTiO_3 slab aligns with the layer polarization in SmNiO_3 partially compensating the $50 \mu\text{C cm}^{-2}$ polar discontinuity. Next, we relax the full superlattice. We find that in this case, SmNiO_3 develops polar displacements of $-20 \mu\text{C cm}^{-2}$ opposite to its layer polarization and the local polarization of BaTiO_3 further reducing the polar discontinuity. In addition, the local polarization in BaTiO_3 reduces slightly (green line). The band bending due to the polar discontinuity disappears upon relaxation (green in Fig. 2a).

We can estimate the remaining interface charges using Eq. 1 and the averaged local polarizations P_{BTO} for the BaTiO_3 and P_{SNO} for the SmNiO_3 slabs:

$$\sigma_{\text{inter}} = 50 \mu\text{C cm}^{-2} + P_{\text{BTO}} - P_{\text{SNO}} \quad (3)$$

We see that by becoming polar, the response of the ions considerably reduces σ_{inter} from $\pm 50 \mu\text{C cm}^{-2}$ to values of only $\pm 7 \mu\text{C cm}^{-2}$ (Table I). Note that Eq. 3 does not account for the redistribution of free charge in metallic SmNiO_3 .

We can therefore estimate that the metallic screening from the SmNiO_3 is of the order of $\pm 7 \mu\text{C cm}^{-2}$, considerably less than the $-20 \mu\text{C cm}^{-2}$ from the polar displacements of the ions. Similarly, Ref. [28] reported that polar displacements over 2-3 formula units in the SrRuO_3 electrode of $\text{BaTiO}_3/\text{SrRuO}_3$ superlattices helped to stabilize a larger ferroelectric polarization in the BaTiO_3 . In contrast to their findings, the polar displacements in our superlattice are uniform across the entire SmNiO_3 slab, although it is unclear whether the polar displacements would remain uniform for thicker slabs.

Interestingly, in the relaxed structure we find a small band bending in BaTiO_3 core states opposite to the field introduced by the layer charges, see Fig. S1. We assign the inverse field to an enhanced polar displacement in the NiO_2^- layer at the BaO/NiO_2 interface caused by steric effects. NiO_2^- is sandwiched between a layer with large Ba^{2+} and small Sm^{3+} ions which induce an off-centering of O^{2-} relative to Ni^{3+} towards Sm^{3+} . Additionally, the O^{2-} are more electrostatically attracted to the Sm^{3+} than the Ba^{2+} further enhancing the local interfacial polar displacement. In $\text{BaTiO}_3/\text{SrRuO}_3$ superlattices, an analogous enhancement of the polarization due to the ion size difference at the BaO/RuO_2 interface has been observed [29]. We will determine in the next section whether this effect is inherent to the superlattice or if it is a consequence of disabling the rotations in the

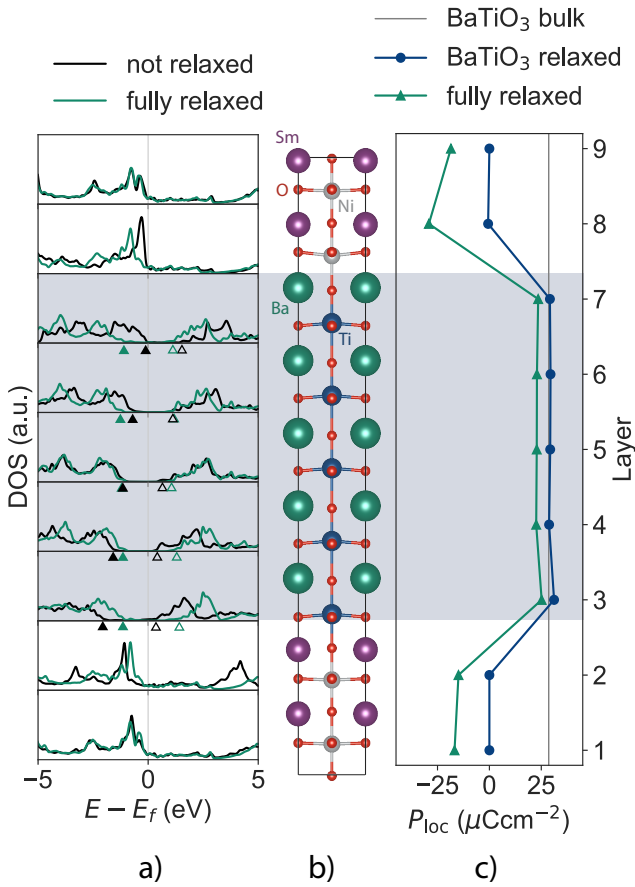


Figure 2: Superlattice without rotations in SmNiO_3 : a) Layer-by-layer DOS for superlattice without (black) and with (green) relaxation. The band shift in BaTiO_3 is indicated by corresponding green and black triangles for the valence band maximum (full) and conduction band minimum (empty). b) Structure of the superlattice after full relaxation. c) Layer-resolved, local polarization ($\mu\text{C cm}^{-2}$) with only the BaTiO_3 layer relaxed (blue) and with relaxation of the full structure (green). The bulk polarization value (vertical gray line) is shown as a reference.

SmNiO_3 .

In conclusion, we find that in the absence of polarization in the BaTiO_3 , clear signatures of an electric field across the BaTiO_3 slab are present in the calculated electronic structure, indicating the incomplete screening of the polar discontinuity by the metallic SmNiO_3 . σ_{inter} is strongly reduced by the spontaneous polarization in BaTiO_3 aligning parallel to the layer polarization within SmNiO_3 , along with additional opposite polar displacements in SmNiO_3 .

Table I: Uncompensated interface charges σ_{inter} as calculated from the response of the ions (Eq. 3) in units of $\mu\text{C cm}^{-2}$.

	non-polar	happy	unhappy
no rotations	± 50	± 7	± 36
with rotations	± 50	± 13	± 53

B. Properties of superlattices with active rotations in SmNiO_3

We continue by comparing our previous results to the case in which SmNiO_3 is allowed to develop octahedral rotations. We again find a band bending in the layer-resolved DOS if we do not relax our superlattice and constrain BaTiO_3 to the cubic symmetry (Fig. 3a in black). As for the case of disabled rotations, the band bending disappears once we fully relax the structure (green in Fig. 3a), and a spontaneous polarization forms in BaTiO_3 aligned with the layer polarization of SmNiO_3 . The corresponding polar displacements of Ti and O are clearly visible in Fig. 3b. We again relax first only the BaTiO_3 slab with SmNiO_3 fixed and the full structure in a second step. The polarization in the BaTiO_3 slab is $20 \mu\text{C cm}^{-2}$ after relaxation of the BaTiO_3 slab and upon full relaxation, it increases to an average polarization of $28 \mu\text{C cm}^{-2}$ which is very close to the bulk polarization value of $29 \mu\text{C cm}^{-2}$. Overall, the response of BaTiO_3 to the polar discontinuity in superlattices with rotations in the SmNiO_3 is analogous to that in the superlattice with disabled rotations.

The octahedral rotations however clearly influence the polar displacements in SmNiO_3 : We find that the average polar displacement of the SmNiO_3 slab reduces from $-20 \mu\text{C cm}^{-2}$ in superlattices with disabled rotations to $-8 \mu\text{C cm}^{-2}$ in superlattices with active octahedral rotations. In the latter structure, the local polar displacement is largest at the upper NiO_2/BaO interface where the octahedral rotations are more suppressed (see Fig. 3b). This behavior is consistent with the hardening of the polar mode that we find on the introduction of the octahedral rotations (see Fig. S3). Octahedral rotations and ferroelectricity often do not coexist in literature and several studies have shown that if the rotations are suppressed, ferroelectricity may emerge in perovskites that are otherwise not ferroelectric [30–32]. Additionally, the steric effects that suppress the rotations at the NiO_2/BaO interface enhance the polar displacements, analogous to the effect we observed in superlattices with disabled rotations.

We have thus shown that the polar discontinuity arising from SmNiO_3 with active rotations leads to a similar BaTiO_3 response as in the superlattice with SmNiO_3 rotations disabled, thus indicating that the contribution of the metallic screening to reducing σ_{inter} is similar for SmNiO_3 with and without rotations. While the behavior

is similar in the two cases, ionic screening in SmNiO_3 is reduced when rotations are active, and consequently, the interface charges of $\pm 13 \mu\text{C cm}^{-2}$ (Table I) are higher.

C. Stability of the polar displacements

In this section, we explore two aspects of the stability of the ‘ferroelectricity’ in BaTiO_3 , first, the critical thickness of the polarization for BaTiO_3 and second, the stability of the unhappy polarization orientation with increasing BaTiO_3 slab thickness.

We begin by calculating the energy as a function of the bulk soft mode distortion for superlattices containing 1, 5, and 10 layers of BaTiO_3 and 4 layers of SmNiO_3 . Our results are shown in Fig. 4a. The soft mode distortion is defined to be the change in structure of bulk BaTiO_3 between the high-symmetry cubic and the polar tetragonal phase. A distortion of 0 thereby corresponds to cubic BaTiO_3 and at the full bulk polarization, the distortion is 1. The superlattices were then constructed from a slab of BaTiO_3 with different fractional distortions and a slab of SmNiO_3 with active rotations, and the energy was calculated without any further structural relaxation.

We first analyze the right-hand side of Fig. 4a, which shows the energy as a function of soft mode distortion in the happy direction. We find a global minimum at +1 soft mode distortion for all three thicknesses down to 1 layer of BaTiO_3 , indicating that these superlattices have no critical thickness. Next, we construct superlattices with 1-5 layers of centrosymmetric BaTiO_3 and 4 layers of SmNiO_3 with active rotations and subsequently relax them. Fig. 5 shows the averaged P_{loc} of the BaTiO_3 slab (green) as a function of slab thickness. We indeed find that the averaged out-of-plane polarization is stable down to a single unit cell and maintains a polarization value close to P_{bulk} of BaTiO_3 (grey dashed line), in contrast to the critical thickness found in BaTiO_3 with SrRuO_3 electrodes [33]. Our findings are consistent with those of Ref. [10], which reported an absence of critical thickness for $\text{BaTiO}_3/\text{LaNiO}_3$ superlattices, and indicate a strong polarizing field created by the interface charges [34].

Next, we focus on the left-hand side of Fig. 4a which corresponds to the unhappy polarization direction where P_{loc} of BaTiO_3 is opposite to P_{layer} of SmNiO_3 . Without any metallic screening, the polar discontinuity in the unhappy orientation would increase up to $\sim \pm 80 \mu\text{C cm}^{-2}$ for P_{loc} of BaTiO_3 with its full bulk polarization value. Hence, we would expect this orientation to be energetically highly disfavored, particularly for very thin BaTiO_3 slabs. In previous studies with $\text{BiFeO}_3/\text{SrRuO}_3$ superlattices, for example, the unhappy polarization orientation of BiFeO_3 in $\text{BiFeO}_3/\text{SrRuO}_3$ superlattices was only metastable for six or more BiFeO_3 layers [8] and the disfavored orientation for $\text{BaTiO}_3/\text{LaNiO}_3$ superlattices could only be stabilized for more than eight BaTiO_3 layers [10].

For five layers of BaTiO_3 , we find no metastable minimum for the unhappy orientation. For thicker layers, a

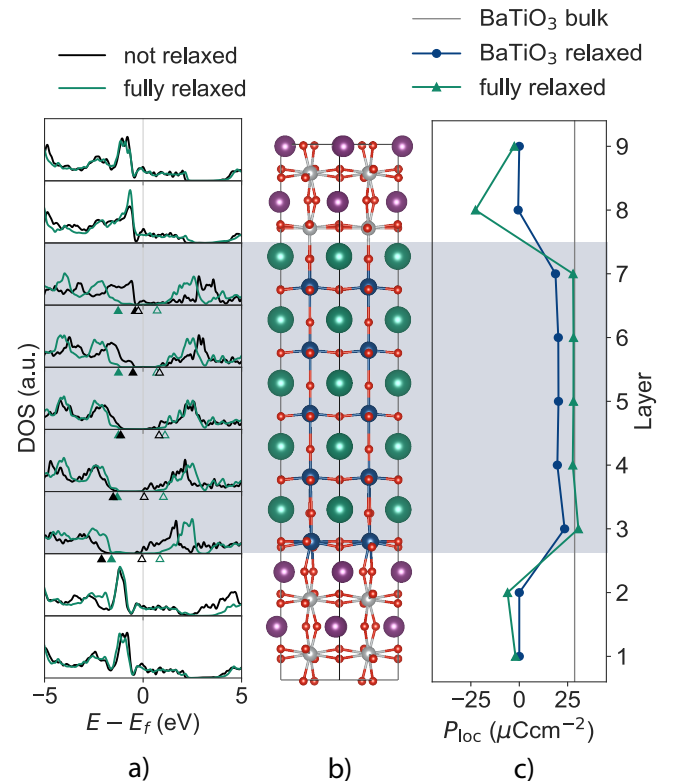


Figure 3: Superlattice with rotations in SmNiO_3 : a) Layer-by-layer DOS for superlattice without (black) and with (green) relaxation. The band shift in BaTiO_3 is indicated by corresponding green and black triangles for the valence band maximum (full) and conduction band minimum (empty). b) Superlattice after full relaxation. c) Layer-resolved, local polarization ($\mu\text{C cm}^{-2}$) with only the BaTiO_3 relaxed (blue) and relaxation of the full structure (green). The bulk polarization value of BaTiO_3 (vertical gray line) is shown as a reference.

local minimum that is $\sim 100 \text{ meV/f.u.}$ higher in energy than that at +1, is found. Therefore, for a large enough number of BaTiO_3 layers, we expect a metastable unhappy state and switchable BaTiO_3 polarization albeit with a strong exchange bias. Note that the minimum for the unhappy orientation appears at -0.8 soft mode distortion, suggesting that we should expect a smaller polarization in this orientation.

We find that superlattices with up to seven layers of BaTiO_3 initialized in the unhappy orientation always reverse the orientation of the BaTiO_3 polarization upon relaxation, resulting in the happy state. We are able to study the unhappy system, however, by fixing the middle 3 layers of BaTiO_3 to $-P_{\text{spont}}$ and relaxing the remaining atoms. The resulting DOS for the superlattice with rotations (purple in Fig. 6a) shows a similar band bending to that of the unrelaxed superlattices with centrosymmetric BaTiO_3 (black in Fig. 2 and 3). The band bending is strong enough to shift the conduction band of the

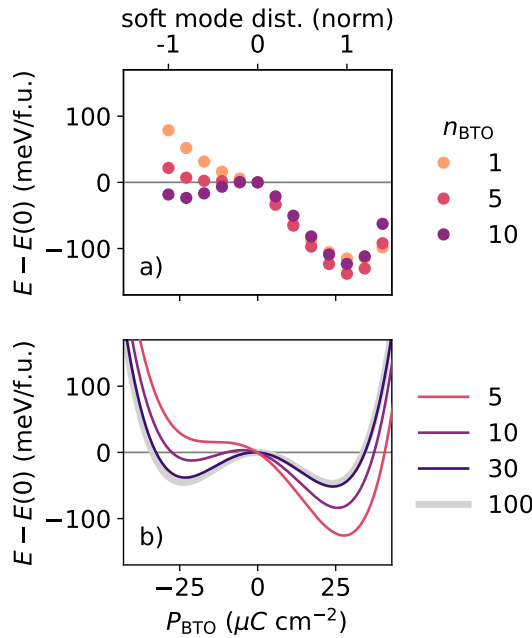


Figure 4: Energy as a function of the polarization for different BaTiO_3 slab thicknesses. The energy zero is set to that of zero BaTiO_3 polarization inside the superlattice and the polar displacements of SmNiO_3 are set to zero for both graphs. a) Energy profile obtained from DFT for $\text{SmNiO}_3/\text{BaTiO}_3$ superlattices with active rotations in the 4 SmNiO_3 layers and $n_{\text{BTO}} = 1, 5, 10$ BaTiO_3 layers. The full DFT polarization of the bulk BaTiO_3 is $P_{\text{BaTiO}_3} = 28.6 \mu\text{C cm}^{-2}$. b) Energy profile obtained from the electrostatic model for superlattices $n_{\text{BTO}} = n_{\text{SNO}} = 5, 10, 30, 100$ layers. The bulk polarization of BaTiO_3 in the electrostatic model is at $P_{\text{BTO}} = 24.0 \mu\text{C cm}^{-2}$.

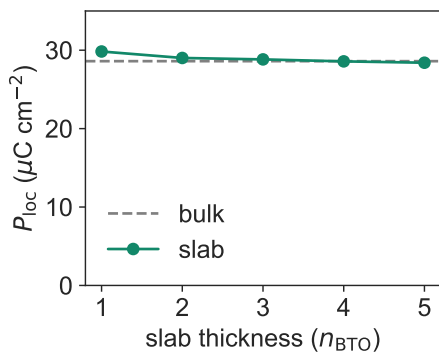


Figure 5: Average BaTiO_3 polarization as a function of BaTiO_3 slab thickness in $(\text{BaTiO}_3)_n(\text{SmNiO}_3)_4$ superlattices in the happy orientation. The spontaneous bulk polarization value of BaTiO_3 is given as a reference (gray dashed line)

BaTiO_3 below the Fermi level at the lower TiO_2/SmO interface, indicating an additional screening mechanism of electrons in the interfacial BaTiO_3 layer. The results for SmNiO_3 with disabled rotations show the same trends (Fig. S2) and, therefore, we restrict our discussion to superlattices with active rotations in the following.

The structures of both SmNiO_3 and BaTiO_3 are affected by the increased polar discontinuity in the unhappy state. BaTiO_3 reduces its local polarization at the interfaces where the atoms are not constrained (Fig. 6c) and, despite the rotations, SmNiO_3 increases its polar displacements. Still, the superlattice is left with σ_{inter} of $\pm 53 \mu\text{C cm}^{-2}$ (Table I), which is considerably smaller than the value in the happy case of $\pm 13 \mu\text{C cm}^{-2}$ and comparable to σ_{inter} of the unrelaxed structures.

In conclusion, we find the unhappy orientation of BaTiO_3 in $\text{SmNiO}_3/\text{BaTiO}_3$ superlattices to be energetically highly disfavored. We are not able to stabilize the unhappy orientation for up to seven layers of BaTiO_3 but expect it to become metastable for a higher slab thickness. The happy orientation however shows a clear stable minimum for all slab thicknesses, allowing an out-of-plane polarization down to a single unit cell with no critical thickness.

D. Electrostatic model

In this last section, we construct an electrostatic model and use it to study the stability of the two polarization states for thick layers with up to 100 unit cells of BaTiO_3 and SmNiO_3 each, which are not accessible within DFT. We also use it to study the effect of various parameters such as the dielectric permittivity and the effective screening length on the behavior to guide possible choices of materials for future work.

The model describes the electrostatics at the interface and the associated energy costs to screen them. The total energy E_{es} consists of the following contributions:

$$E_{\text{es}} = E_{P,\text{BTO}} \cdot d_{\text{BTO}} + E_{P,\text{SNO}} \cdot d_{\text{SNO}} + E_{\text{d}} + E_{\text{scr}} \quad (4)$$

Here, $E_{P,\text{BTO}}$ and $E_{P,\text{SNO}}$ are the energies needed to polarize the BaTiO_3 and SmNiO_3 slabs of respective thicknesses d_{BTO} and d_{SNO} [34, 35], E_{d} is the electrostatic cost resulting from the imperfect screening of the interface charge σ_{inter} by the metallic electrons in the electrode [36, 37] and E_{scr} is the cost associated with possible additional screening via electron-hole excitation across the band gap [34, 35]. We describe the electrostatic model in more detail in the appendix.

We estimate $E_{P,\text{BTO}}$ and $E_{P,\text{SNO}}$ from the energy profiles of bulk BaTiO_3 and SmNiO_3 (Fig. S3), obtained by displacing the atoms according to the lowest frequency polar phonon mode of the tetragonal centrosymmetric structure. BaTiO_3 shows the characteristic double-well potential with minima at $\pm 24 \mu\text{C cm}^{-2}$ (note that this value is slightly lower than the relaxed bulk polarization). SmNiO_3 is lowest in energy at zero polarization, with the

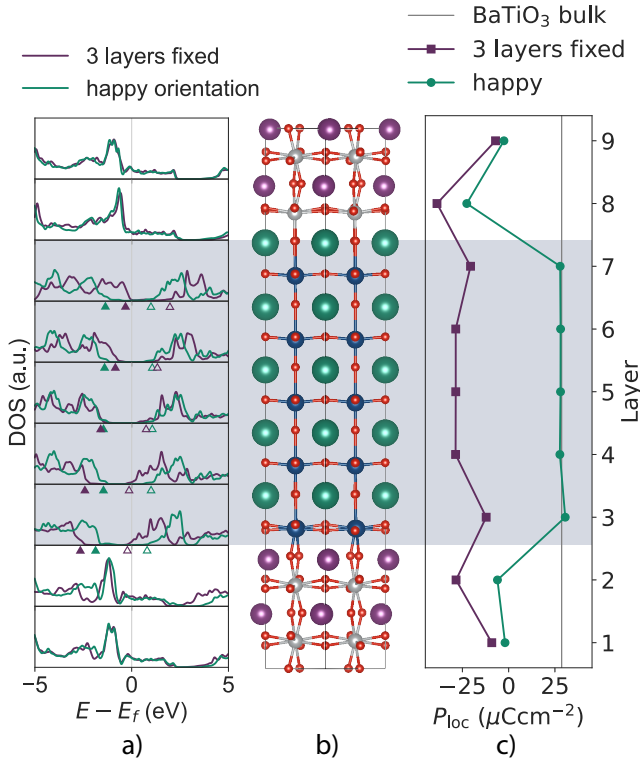


Figure 6: Unhappy superlattice with three fixed BaTiO₃ layers: a) Local DOS of the happy superlattice from Fig. 3 (green) and superlattice with three BaTiO₃ layers fixed to the unhappy orientation (purple). The band shift in BaTiO₃ is indicated by corresponding green and purple triangles for the valence band maximum (full) and conduction band minimum (empty). b) Superlattice after relaxation with 3 fixed layers. c) Layer-resolved, local polarization ($\mu\text{C cm}^{-2}$) for relaxation with the unhappy, fixed BaTiO₃ layers (purple) and for the relaxed happy structure from Fig. 3 (green).

energy increasing particularly rapidly with polarization when rotations are active. This highlights again the importance of correctly treating the rotations in SmNiO₃.

1. Fit and extrapolation to larger slab thicknesses

We fit the model to our DFT calculations for $(\text{BaTiO}_3)_n(\text{SmNiO}_3)_4$ ($n = 5, 10, 30$) to extract the physics of the following three parameters: the band gap of BaTiO₃, the dielectric constant ϵ_r of BaTiO₃, and the effective metallic screening length λ_{fit} . The band gap linearly determines the energy cost of screening by electron-hole excitations (Eq. S6) and the energy of the depolarizing field is proportional to the ratio $\lambda_{\text{fit}}^2/\epsilon_r$ (Eq. S5). We find good agreement for the shape of the energy profiles between DFT and the model for $\lambda_{\text{fit}}^2/\epsilon_r = 1 \times 10^{-19} \text{ m}^2$ at the experimental band gap of 3.2 eV [38, 39] (Fig. S4). We discuss the physical meaning and validity of these

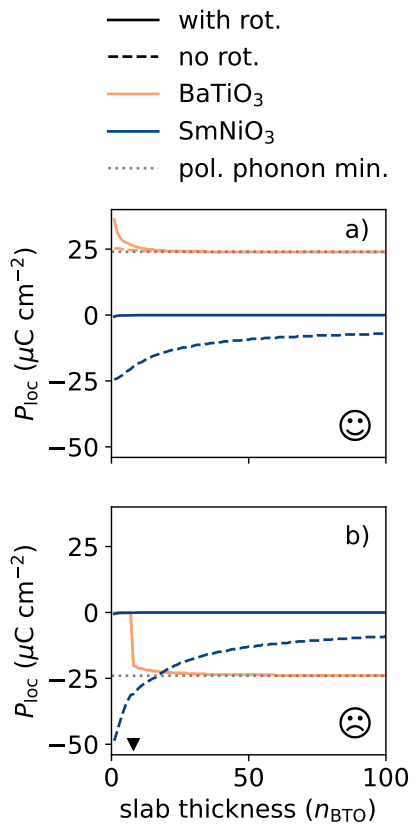


Figure 7: Local polarization for BaTiO₃ (yellow) and polar displacements for SmNiO₃ (blue) with active (full line) and disabled (dashed line) rotations in the SmNiO₃ as a function of slab thickness in formula units ($n_{\text{BTO}} = n_{\text{SNO}}$) as obtained from the electrostatic model. a) Happy and b) unhappy orientation of BaTiO₃ in the superlattice. The polarization of BaTiO₃ at $24.0 \mu\text{C cm}^{-2}$ obtained from freezing in the lowest-energy polar phonon displacements is shown as a comparison (dotted gray). The unhappy orientation has an energy minimum for 8 and more f.u. of BaTiO₃ (black triangle).

values later.

Next, we use the model with the fitted parameters to calculate the evolution of the energy and polarization of the happy and unhappy phases for larger slab thicknesses, and show the calculated energy profiles in Fig. 4 and the resulting polarizations in Fig. 7. Fig. 4 compares the energy profiles from DFT (a) with the results from the electrostatic models (b) for zero polar displacements in SmNiO₃. As imposed by the fit of $\lambda_{\text{fit}}^2/\epsilon_r$, a metastable minimum appears for the unhappy orientation between a slab thickness of 5 and 10 formula units. Extending to thicker slabs in the electrostatic model, we see the two minima of the double well potential become closer in energy as thickness is increased until the energy differences between them are less than 15 meV/f.u. for 30 and negligibly small ($\sim 1 \text{ meV/f.u.}$) for 100 layers of BaTiO₃.

This is a result of the expected reduced influence of the polar discontinuity as the slab thickness is increased.

Fig. 7a shows the corresponding size of the local polar displacements for the happy orientation in superlattices of BaTiO₃ (orange) and SmNiO₃ (blue) with active (full line) and disabled (dashed line) rotations up to 100 layers. Not surprisingly, the polar displacement of SmNiO₃ with active rotations at one unit cell of SmNiO₃ is less than 1 $\mu\text{C cm}^{-2}$ and disappears completely for thicker SmNiO₃ slabs. Consequently, BaTiO₃ mainly compensates the polar discontinuity, resulting in a polarization of 36 $\mu\text{C cm}^{-2}$ in a BaTiO₃ slab of one unit cell thickness. Note that this value is higher than the bulk polarization of BaTiO₃, and that it reduces the remaining interface charge to 13 $\mu\text{C cm}^{-2}$, which is to be screened by the metal and electron-hole excitations. For SmNiO₃ with disabled rotations, a considerable polar displacement in SmNiO₃ is present even for thick slabs. The polar displacement in SmNiO₃ reduces from 24 $\mu\text{C cm}^{-2}$ at 1 f.u. to a value of 6 $\mu\text{C cm}^{-2}$ at 100 f.u. while P_{BTO} is close to that of the soft mode minimum for all thicknesses. As previously observed in our DFT calculations, we do not see a critical thickness for the BaTiO₃ polarization.

Since the unhappy orientation is not even metastable up to 7 layers, we see in Fig. 7b that the polarization of BaTiO₃ remains zero up to this thickness. Once the unhappy orientation becomes metastable, P_{loc} jumps from zero to $-20 \mu\text{C cm}^{-2}$ at 8 BaTiO₃ layers, corresponding to the formation of the local minimum that we found within DFT. Interestingly, we see that the polarizations of BaTiO₃ in superlattices with active and disabled tilts coincide. The additional polar displacements in SmNiO₃ with disabled rotations do not influence the thickness needed to form a metastable minimum even though the absence of rotations reduces the energy difference between the two polarization orientations (see Fig. S5). This apparently counterintuitive finding is a consequence of the fact that, in the unhappy orientation, any polarization of BaTiO₃ increases the polar discontinuity. The formation of a metastable minimum is therefore only possible when the energy gain on polarizing BaTiO₃ exceeds the cost of increasing the polar discontinuity. In our model, both costs only depend on the BaTiO₃ and therefore, we observe the formation of a local minimum for the same slab thickness in superlattices with active and disabled SmNiO₃ rotations. The happy and unhappy orientations in Fig. 7 converge to the same absolute polarization value for thick slabs, confirming that the unhappy orientation is less energetically disfavored for thick BaTiO₃.

2. Influence of different parameters on the ferroelectric properties

Next, we will study the effect of varying the dielectric permittivity, the metallic screening, and the electron-hole excitations across the band gap on the ferroelectric prop-

erties of the BaTiO₃ layer. In particular, by changing the metallic screening, we are able to mimick a metal-to-insulator transition (MIT) in the electrode. For $\gamma = \frac{2\lambda_{\text{fit}}}{d_{\text{BTO}}}$ close to zero (small screening length) the electrode is a very good metal, at intermediate γ it is a poor metal and when $\gamma = 1$ we obtain the fully insulating state.

Fig. 8 shows the calculated energy as a function of the BaTiO₃ polarization across the MIT with $\gamma = 0.1$ (yellow), 0.5 (pink) and 1 (purple) for $\epsilon_r = 1$ (a), 30 (b) and 90 (c) and a slab thickness $d_{\text{BTO}} = d_{\text{SNO}} = 8$ unit cells. We compare the results with allowed (full line) and excluded (dashed line) additional screening by electron-hole excitation across the BaTiO₃ band gap.

We can make the following conclusions from comparing the different plots: First, the additional carriers from electron-hole excitations strongly influence the stability of the unhappy orientation when the screening in the metal is poor and the dielectric permittivity in the ferroelectric is low. For low dielectric permittivities, the unhappy orientation is highly disfavored without screening by forming additional charge carriers (dashed line) in both the insulating and intermediate metallicity electrode cases. When the metallic screening is improved, fewer charge carrier excitations across the gap are needed and for the most metallic case, there are no electron-hole excitations present even at low ϵ_r . Second, a larger ϵ_r reduces the effect of the polar discontinuity and decreases the energy difference between the two polarization orientations. The double well of the insulating case (purple) does not change much with ϵ_r , and the unhappy orientation is disfavored even for $\epsilon_r = 90$. For intermediate screening (pink), the double well potential is the most sensitive to ϵ_r . At $\epsilon_r = 1$, the intermediate screening and the most insulating case (purple) coincide while at $\epsilon_r = 90$, the intermediate screening is close to the most metallic case (yellow). For the most metallic case (yellow), the energy difference between the happy and unhappy orientation is negligible for $\epsilon_r = 90$, restoring the typical ferroelectric double well potential. Lastly, the energy difference between the happy and unhappy orientations increases for all cases as the system becomes more insulating, destabilizing the unhappy polarization orientation. For $\epsilon_r = 1$, both the insulating and intermediate metallicity electrodes cannot stabilize the unhappy orientation, and only the most metallic system (yellow curve) shows a metastable minimum. For $\epsilon_r = 30$, the intermediate screening leads to moderate stabilization of the unhappy orientation while a good screening significantly stabilizes the unhappy orientation. For $\epsilon_r = 90$, we again see that intermediate screening already results in the unhappy orientation being stable.

These results show that a change in the metallic screening length, as occurs across a MIT, can significantly alter the relative stabilities of the two polarization states. The changes across a MIT in the ferroelectric double well potential are most significant for higher dielectric susceptibilities and if the electrode has good screening in the metallic state. The destabilization of the unhappy

orientation on changing from metallic to an insulating electrode as found for $\epsilon_r = 90$ (Fig. 8c) could be significant enough to lead to switching from the unhappy to the happy orientation when the electrode changes from metallic to insulating.

In general, high ϵ_r and good metallic screening minimize the effects of the polar discontinuity on the ferroelectric. Thus if a metal with charged layers is to be used as a simple electrode, care should be taken to select one with those properties. Increasing the ferroelectric slab thickness additionally improves the switchability and reduces the impact of the polar discontinuity. To build a ferroelectric device that exploits the polar discontinuity, for example with a strong exchange bias, on the other hand, we recommend a low dielectric susceptibility and a metal with bad screening capabilities. Again, adjusting the film thickness controls the extent of the bias, with thinner BaTiO₃ films leading to unidirectional behavior.

3. Physical relevance of the parameters

Lastly, we discuss the physical values and best estimates of the parameters ϵ_r and E_g for BaTiO₃ and the effective screening length for SmNiO₃.

We start with the metallic screening length, which we extract in three different ways from our DFT calculations. First, we estimate the Thomas-Fermi screening length, which assumes that the electrons behave as a free-electron gas, and is given by

$$\lambda_{\text{TF}} = \left(\frac{e^2}{\epsilon_0} D(\epsilon_F) \right)^{-1/2}, \quad (5)$$

where $D(\epsilon_F)$ is the DOS at the fermi level and e is the electronic charge [40]. For our calculation of relaxed bulk SmNiO₃ with active rotations, we obtain $D(\epsilon_F) = 2.1 \times 10^{17} \text{ states}/\text{\AA}^3$ and λ_{TF} to be 0.4 \AA . We note that, for a correlated metal such as SmNiO₃, this is likely to be an underestimate, since the density of states in such systems tends to be high and the electrons rather localized and less able to contribute to screening than in the free-electron case. Second, we convert the change in potential ΔV induced by the electric field across the BaTiO₃ slab to a screening length λ_{DOS} using the relation [37]

$$\lambda_{\text{DOS}} = \frac{1}{2} \epsilon_0 \epsilon_r \frac{\Delta V}{\sigma_{\text{inter}}}. \quad (6)$$

We extract ΔV from the BaTiO₃ core-state shift of the states between -29 eV and -24 eV in the DOS in a superlattice containing five layers of BaTiO₃ and 4 layers of SmNiO₃ frozen in their high-symmetry paraelectric atomic positions (Fig. S1) rather than from the step in the macroscopically averaged electrostatic potential used in previous studies [28, 33, 41]. When we set $\epsilon_r = 1$ in Eq. 6, as was usually done in previous studies [5, 28, 33], we obtain $\lambda_{\text{DOS}} = 0.2 \text{ \AA}$, and for the DFT value of

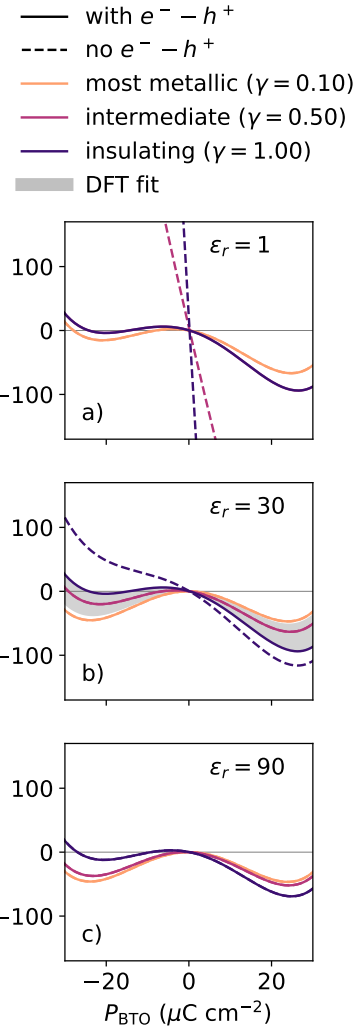


Figure 8: Energy versus polarization across the metal-to-insulator transition for $\epsilon_r = 1, 30$ and 90 and slab thickness of $d = 8$ formula units for both SmNiO₃ and BaTiO₃. The MIT is mimicked by changing from a very short screening length $\gamma = 0.1$ ($\lambda_{\text{fit}} = 1.67 \text{ \AA}$) to a fully insulating system with $\gamma = 1$ ($\lambda_{\text{fit}} = 16.70 \text{ \AA}$). Results for models with allowed (full line) and forbidden (dashed line) electron-hole excitation across the band gap are shown. The polar displacements of SmNiO₃ are zero for all curves. For $\epsilon_r = 30$ (b), the energy range spanned by λ_{DOS} and λ_{fit} , extracted from DFT using different methods, are superimposed in gray.

$\epsilon_r = 6$ [42] the corresponding screening length is 1.1 \AA , almost triple the screening length from the Thomas-Fermi model. We emphasize that, in this comparison, the slab calculation was performed with the ions frozen in their high-symmetry structures, so the difference can not be attributed to screening via ionic relaxations.

Lastly, we can estimate λ_{fit} from the ratio $\lambda_{\text{fit}}^2/\epsilon_r = 1 \times 10^{-19} \text{ m}^2$ obtained from fitting the electrostatic model. Here it is less clear what value to assume for ϵ_r . For

$\epsilon_r = 1$, the ratio corresponds to $\lambda_{\text{fit}} = 3.2 \text{ \AA}$, for the high frequency DFT value $\epsilon_r = 6$, it is 7.7 \AA and for $\epsilon_r = 60$ (experimental literature values at room temperature vary between 60-110 [43–46]), we obtain a screening length of 24.5 \AA . This λ_{fit} is considerably larger again than the two previously extracted screening lengths λ_{DOS} and λ_{TF} , indicating that poor metallic screening in the model best reproduces the DFT behavior. The large λ_{fit} is likely a consequence of the model capturing the high lattice response of the DFT calculations; we emphasize also that interfacial effects such as changes in chemical bonding at the interface are completely neglected in the model. In Fig. 8, we show again the energy versus polarization of Figure 4b for $\epsilon_r = 30$ and eight layers each of SmNiO_3 and BaTiO_3 , superimposing in gray the physically plausible metallic screening range spanned by λ_{DOS} (low-energy limit) and λ_{fit} (high-energy limit).

Next, we discuss the value of the BaTiO_3 band gap in the electrostatic model. Surprisingly, the experimental band gap of 3.2 eV provides a better model fit to our DFT-calculated energy versus polarization for the superlattices than the DFT band gap of 1.8 eV . This is likely because effects such as interfacial chemical bonding and octahedral tilt coherence in the DFT calculations alleviate the impact of the polar discontinuity and reduce the need for electron-hole screening. Since such effects are not included in the electrostatic model, the reduction is renormalized into a reduced screening by electron-hole excitations associated with the larger band gap.

To summarize this section, we find that the simple electrostatic model of Eq. 4 can reproduce the energy profiles over the range of thicknesses accessible in DFT calculations for thin films and can be conveniently used to extrapolate to larger slab thicknesses. We confirm that, as expected, the energy difference between happy and unhappy orientations is reduced in thicker films, becoming negligibly small for 30 formula units. In addition, our model allows us to test the effects of various parameters, such as the metallic screening length, on the properties of the superlattices, providing a simple and useful tool for studying how parameters such as slab thickness and metallic screening length affect the system's behavior. In particular, we find that the metallic screening length strongly influences the (meta)-stability of the unhappy BaTiO_3 orientation. This raises the interesting question of whether, in addition to the metallicity of the electrode affecting the polarization of the ferroelectric, the reciprocal behavior might occur, and the orientation of the ferroelectric polarization might affect the metallicity of the electrode. We envisage a scenario in which the superlattice layer thicknesses and materials are selected so that the electrode is insulating, and close to the metal-insulator transition when the ferroelectric is in its happy orientation. Switching the ferroelectric into its unhappy orientation could then force a transition of the electrode to the metallic state. Detailed electronic structure calculations for thicker slabs and at finite temperature would be helpful in identifying suitable material combinations

and geometries.

IV. CONCLUSION

In summary, we have shown that the layer polarization in a metal can strongly affect the spontaneous polarization of the ferroelectric layer in metal-ferroelectric superlattices.

We confirmed that in $\text{SmNiO}_3/\text{BaTiO}_3$ superlattices the charge carriers in metallic SmNiO_3 cannot sufficiently screen its own layer polarization, and consequently, BaTiO_3 compensates for the polar discontinuity by orienting its spontaneous polarization parallel to the layer polarization of SmNiO_3 . This out-of-plane spontaneous BaTiO_3 polarization stays stable down to a single unit cell, with no critical thickness for the ferroelectric thin films in this superlattice. Similarly to other systems with polar discontinuities [8, 10], the unhappy direction which increases the polar discontinuity and the interface charge is highly disfavored and BTO thicknesses up to seven layers do not even have a high energy metastable minimum for the unhappy direction. Based on the energy as a function of the soft mode distortion, we would expect the unhappy orientation to be metastable in thicker films.

We find that the inability of SmNiO_3 to fully screen the polar discontinuity is independent of whether its rotations are active or disabled. The lattice response is, however, different for the two cases and when the octahedral rotations are not taken into account, the ability of SmNiO_3 to form polar distortions is drastically overestimated.

We constructed an electrostatic model incorporating the energy lowering of forming a polarization in BaTiO_3 and partially screening the interfacial charges by the metallicity of the electrode, and the costs of forming polar displacements in SmNiO_3 , having a polar discontinuity and forming additional screening charges by electron-hole excitation. The model recreates our DFT behavior at low slab thicknesses and confirms that increasing the film thickness reduces the energy difference between the two polarization orientations. By varying our model parameters, we found that a shorter metallic screening length and a higher dielectric permittivity stabilize the unhappy orientation, indicating that a MIT could influence the ferroelectric switching behavior. This raises the question of whether, analogously, switching the ferroelectric could induce a MIT. If the ferroelectric is forced to the unhappy orientation in the insulating state of the electrode, the material would need to compensate for the increased interface charges. It could either stabilize by electron-hole excitations across the gap or by transitioning back to the metallic state. If the material is very close to the MIT temperature and the metallic screening length is short enough, the additional energy lowering could tip the material into transitioning to the metallic state. Studying the influence of the polar discontinuity

on the MIT could be an interesting direction for future research.

Using the model, we studied the influence of different model parameters on the ferroelectric double well potentials. While the model is good at predicting general trends, it is not well-suited to get more quantitative results as there is a significant spread in realistic parameter values. Therefore, it is not clear how the ferroelectric states of $\text{SmNiO}_3/\text{BaTiO}_3$ superlattices would change upon the MIT.

In conclusion, ferroelectric switching can be controlled in novel ways when using an electrode that both has a layer polarization and can undergo a MIT, though SmNiO_3 may not be ideal for this application. SmNiO_3 is most suitable as an electrode in devices requiring a strong exchange bias. The film thickness can be adjusted to

control the extent of the bias, with thinner BaTiO_3 films leading to unidirectional behavior. If a good switching behavior is required with SmNiO_3 as an electrode, we recommend using a ferroelectric with a high dielectric constant or thick ferroelectric films.

We hope that our predictions inspire experimental work in these directions, both for fundamental research and for device applications.

ACKNOWLEDGMENTS

We thank Morgan Trassin and Ipek Efe for the helpful discussions. This work was supported by the Swiss National Science Foundation under the grant No. 209454 and by ETH Zurich. The calculations for this work were performed on the ETH Zurich Euler cluster.

[1] V. Garcia and M. Bibes, Ferroelectric tunnel junctions for information storage and processing, *Nature Communications* **5**, 4289 (2014).

[2] J. F. Scott, *Ferroelectric Memories*, edited by K. Itoh and T. Sakurai, Springer Series in Advanced Microelectronics, Vol. 3 (Springer Berlin Heidelberg, Berlin, Heidelberg, 2000).

[3] C. A. F. Vaz, Y. J. Shin, M. Bibes, K. M. Rabe, F. J. Walker, and C. H. Ahn, Epitaxial ferroelectric interfacial devices, *Applied Physics Reviews* **8**, 041308 (2021).

[4] Y. Jiang, E. Parsonnet, A. Qualls, W. Zhao, S. Susarla, D. Pesquera, A. Dasgupta, M. Acharya, H. Zhang, T. Gosavi, C.-C. Lin, D. E. Nikonov, H. Li, I. A. Young, R. Ramesh, and L. W. Martin, Enabling ultra-low-voltage switching in BaTiO_3 , *Nature Materials* **21**, 779 (2022).

[5] K. M. Rabe, C. H. Ahn, and J.-M. Triscone, eds., *Physics of Ferroelectrics: A Modern Perspective*, Topics in Applied Physics No. v. 105 (Springer, Berlin ; New York, 2007).

[6] M. Stengel, Electrostatic stability of insulating surfaces: Theory and applications, *Physical Review B* **84**, 205432 (2011).

[7] I. Efe, N. A. Spaldin, and C. Gattinoni, On the happiness of ferroelectric surfaces and its role in water dissociation: The example of bismuth ferrite, *The Journal of Chemical Physics* **154**, 024702 (2021).

[8] N. A. Spaldin, I. Efe, M. D. Rossell, and C. Gattinoni, Layer and spontaneous polarizations in perovskite oxides and their interplay in multiferroic bismuth ferrite, *The Journal of Chemical Physics* **154**, 154702 (2021).

[9] P. Yu, W. Luo, D. Yi, J. X. Zhang, M. D. Rossell, C.-H. Yang, L. You, G. Singh-Bhalla, S. Y. Yang, Q. He, Q. M. Ramasse, R. Erni, L. W. Martin, Y. H. Chu, S. T. Pantelides, S. J. Pennycook, and R. Ramesh, Interface control of bulk ferroelectric polarization, *Proceedings of the National Academy of Sciences* **109**, 9710 (2012).

[10] L. L. Tao and J. Wang, Ferroelectricity and tunneling electroresistance effect driven by asymmetric polar interfaces in all-oxide ferroelectric tunnel junctions, *Applied Physics Letters* **108**, 062903 (2016).

[11] Y.-Z. Wu, H.-S. Lu, T.-Y. Cai, and S. Ju, Interface control of ferroelectricity in $\text{LaNiO}_3\text{-BaTiO}_3$ superlattices, *AIP Advances* **4**, 087109 (2014).

[12] A. Malashevich, M. S. J. Marshall, C. Visani, A. S. Disa, H. Xu, F. J. Walker, C. H. Ahn, and S. Ismail-Beigi, Controlling Mobility in Perovskite Oxides by Ferroelectric Modulation of Atomic-Scale Interface Structure, *Nano Letters* **18**, 573 (2018).

[13] G. H. Kwei, A. C. Lawson, S. J. L. Billinge, and S. W. Cheong, Structures of the ferroelectric phases of barium titanate, *The Journal of Physical Chemistry* **97**, 2368 (1993).

[14] J. Rodríguez-Carvajal, S. Rosenkranz, M. Medarde, P. Lacorre, M. T. Fernandez-Díaz, F. Fauth, and V. Trounov, Neutron-diffraction study of the magnetic and orbital ordering in $^{154}\text{SmNiO}_3$ and $^{153}\text{EuNiO}_3$, *Physical Review B* **57**, 456 (1998).

[15] P. Lacorre, J. Torrance, J. Pannetier, A. Nazzal, P. Wang, and T. Huang, Synthesis, crystal structure, and properties of metallic PrNiO_3 : Comparison with metallic NdNiO_3 and semiconducting SmNiO_3 , *Journal of Solid State Chemistry* **91**, 225 (1991).

[16] G. Kresse and J. Furthmüller, Efficiency of ab-initio total energy calculations for metals and semiconductors using a plane-wave basis set, *Computational Materials Science* **6**, 15 (1996).

[17] G. Kresse and J. Furthmüller, Efficient iterative schemes for *ab initio* total-energy calculations using a plane-wave basis set, *Physical Review B* **54**, 11169 (1996).

[18] J. P. Perdew, A. Ruzsinszky, G. I. Csonka, O. A. Vydrov, G. E. Scuseria, L. A. Constantin, X. Zhou, and K. Burke, Restoring the Density-Gradient Expansion for Exchange in Solids and Surfaces, *Physical Review Letters* **100**, 136406 (2008).

[19] P. E. Blöchl, Projector augmented-wave method, *Physical Review B* **50**, 17953 (1994).

[20] G. Kresse and D. Joubert, From ultrasoft pseudopotentials to the projector augmented-wave method, *Physical Review B* **59**, 1758 (1999).

[21] R. Wahl, D. Vogtenhuber, and G. Kresse, SrTiO_3 and BaTiO_3 revisited using the projector augmented wave

method: Performance of hybrid and semilocal functionals, *Physical Review B* **78**, 104116 (2008).

[22] Monkhorst, Hendrik J. and Pack, James D., Special points for Brillouin-zone integrations, *Phys. Rev. B* **13**, 5188 (1976).

[23] A. Ganose, J. Riebesell, J. George, J. Shen, A. S. Rosen, A. A. Naik, nwinner, M. Wen, rdguha1995, M. Kuner, G. Petretto, M. Horton, Z. Zhu, H. Sahasrabuddhe, A. Kaplan, J. Schmidt, C. Ertural, R. Kingsbury, M. McDermott, R. Goodall, T. Purcell, A. Bonkowski, D. Zügner, and J. Qi, *Materialsproject/atomate2: V0.1.14*, Zenodo (2024).

[24] A. Togo, First-principles Phonon Calculations with Phonopy and Phono3py, *Journal of the Physical Society of Japan* **92**, 012001 (2023).

[25] A. Togo, L. Chaput, T. Tadano, and I. Tanaka, Implementation strategies in phonopy and phono3py, *Journal of Physics: Condensed Matter* **35**, 353001 (2023).

[26] Y.-H. Tang and M.-H. Tsai, Ferroelectric properties of nanometer-scale barium titanate films from first principles, *Journal of Applied Physics* **103**, 034305 (2008).

[27] M. S. J. Marshall, A. Malashevich, A. S. Disa, M.-G. Han, H. Chen, Y. Zhu, S. Ismail-Beigi, F. J. Walker, and C. H. Ahn, Conduction at a Ferroelectric Interface, *Physical Review Applied* **2**, 051001 (2014).

[28] G. Gerra, A. K. Tagantsev, N. Setter, and K. Parlinski, Ionic Polarizability of Conductive Metal Oxides and Critical Thickness for Ferroelectricity in BaTiO₃, *Physical Review Letters* **96**, 107603 (2006).

[29] X. Liu, Y. Wang, P. V. Lukashev, J. D. Burton, and E. Y. Tsymbal, Interface dipole effect on thin film ferroelectric stability: First-principles and phenomenological modeling, *Physical Review B* **85**, 125407 (2012).

[30] D. I. Bilc and D. J. Singh, Frustration of Tilts and A-Site Driven Ferroelectricity in KNbO₃ - LiNbO₃ Alloys, *Physical Review Letters* **96**, 147602 (2006).

[31] T. H. Kim, D. Puggioni, Y. Yuan, L. Xie, H. Zhou, N. Campbell, P. J. Ryan, Y. Choi, J.-W. Kim, J. R. Patzner, S. Ryu, J. P. Podkaminer, J. Irwin, Y. Ma, C. J. Fennie, M. S. Rzchowski, X. Q. Pan, V. Gopalan, J. M. Rondinelli, and C. B. Eom, Polar metals by geometric design, *Nature* **533**, 68 (2016).

[32] N. A. Benedek and C. J. Fennie, Why Are There So Few Perovskite Ferroelectrics?, *The Journal of Physical Chemistry C* **117**, 13339 (2013).

[33] J. Junquera and P. Ghosez, Critical thickness for ferroelectricity in perovskite ultrathin films, *Nature* **422**, 506 (2003).

[34] C. Gattinoni and N. A. Spaldin, Prediction of a strong polarizing field in thin film paraelectrics, *Physical Review Research* **4**, L032020 (2022).

[35] J. A. Mundy, B. F. Grossko, C. A. Heikes, D. Ferenc Segedin, Z. Wang, Y.-T. Shao, C. Dai, B. H. Goodge, Q. N. Meier, C. T. Nelson, B. Prasad, F. Xue, S. Ganschow, D. A. Muller, L. F. Kourkoutis, L.-Q. Chen, W. D. Ratcliff, N. A. Spaldin, R. Ramesh, and D. G. Schlom, Liberating a hidden antiferroelectric phase with interfacial electrostatic engineering, *Science Advances* **8**, eabg5860 (2022).

[36] P. Chandra and P. B. Littlewood, A Landau Primer for Ferroelectrics, in *Physics of Ferroelectrics*, Vol. 105 (Springer Berlin Heidelberg, Berlin, Heidelberg, 2007) pp. 69–116.

[37] C. Lichtensteiger, M. Dawber, and J.-M. Triscone, Ferroelectric Size Effects, in *Physics of Ferroelectrics*, Vol. 105 (Springer Berlin Heidelberg, Berlin, Heidelberg, 2007) pp. 305–338.

[38] S. H. Wemple, Polarization Fluctuations and the Optical-Absorption Edge in BaTiO₃, *Physical Review B* **2**, 2679 (1970).

[39] J. Nowotny and M. Rekas, Defect structure, electrical properties and transport in barium titanate. III. Electrical conductivity, thermopower and transport in single crystalline BaTiO₃, *Ceramics International* **20**, 225 (1994).

[40] C. Kittel, *Introduction to Solid State Physics*, 8th ed. (Wiley, Hoboken, NJ, 2005).

[41] A. Baldereschi, S. Baroni, and R. Resta, Band Offsets in Lattice-Matched Heterojunctions: A Model and First-Principles Calculations for GaAs/AlAs, *Physical Review Letters* **61**, 734 (1988).

[42] Philippe Ghosez, *First-Principles Study of the Dielectric and Dynamical Properties of Barium Titanate*, Ph.D. thesis, Université catholique de Louvain, Louvain-la-Neuve (1997).

[43] A. V. Turik and N. B. Shevchenko, Dielectric spectrum of BaTiO₃ single crystals, *physica status solidi (b)* **95**, 585 (1979).

[44] D. Berlincourt and H. Jaffe, Elastic and Piezoelectric Coefficients of Single-Crystal Barium Titanate, *Physical Review* **111**, 143 (1958).

[45] M. Zgonik, P. Bernasconi, M. Duelli, R. Schlessler, P. Günter, M. H. Garrett, D. Rytz, Y. Zhu, and X. Wu, Dielectric, elastic, piezoelectric, electro-optic, and elasto-optic tensors of BaTiO₃ crystals, *Physical Review B* **50**, 5941 (1994).

[46] O. Nakao, K. Tomomatsu, S. Ajimura, A. Kurosaka, and H. Tominaga, Influence of 180° domains on ferroelectric properties of BaTiO₃ single crystal, *Applied Physics Letters* **61**, 1730 (1992).

Appendix

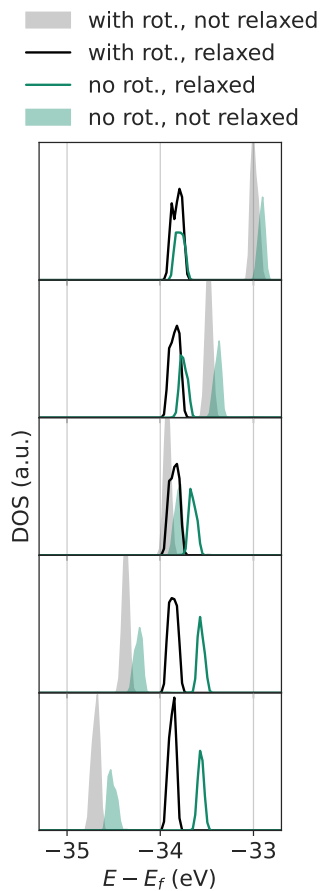


Figure S1: Layer-resolved DOS for BaTiO₃ core-states for superlattice with active (black) and disabled (green) rotations that were either not relaxed (area) or fully relaxed (line).

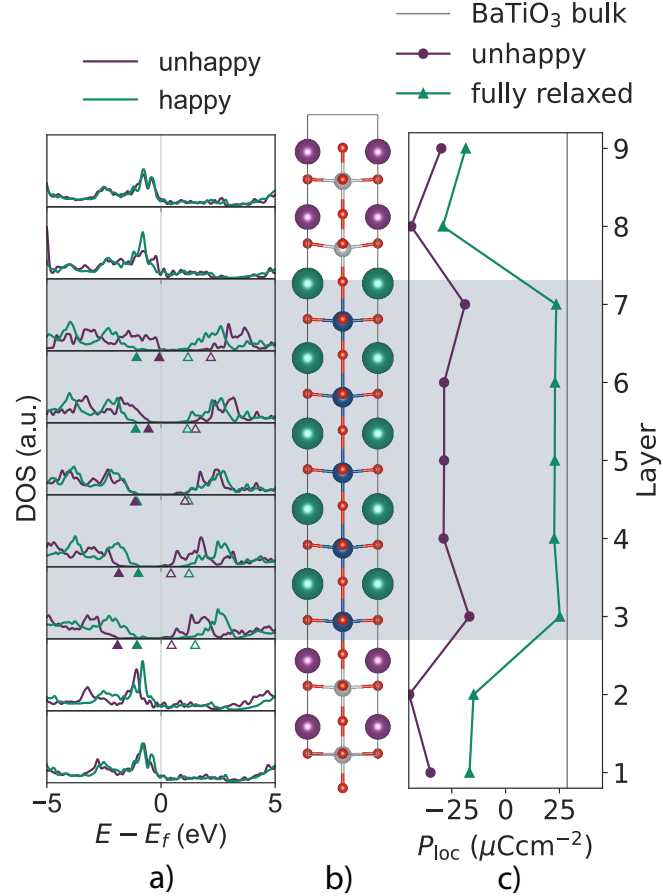


Figure S2: Unhappy superlattice with three fixed BaTiO₃ layers and disabled rotations in SmNiO₃: a) Local DOS of the happy superlattice from Fig. 2 (green) and superlattice with three BaTiO₃ layers fixed to the unhappy orientation (purple). The band shift in BaTiO₃ is indicated by corresponding green and purple triangles for the valence band maximum (full) and conduction band minimum (empty). b) Superlattice after relaxation with 3 fixed layers. c) Layer-resolved, local polarization ($\mu\text{C cm}^{-2}$) for relaxation with the fixed BaTiO₃ layers (purple) and for the relaxed happy structure from Fig. 2 (green).

Electrostatic model

The total electrostatic energy E_{es} per unit surface area of our system is given by

$$E_{\text{es}} = E_{P,\text{BTO}} \cdot d_{\text{BTO}} + E_{P,\text{SNO}} \cdot d_{\text{SNO}} + E_{\text{d}} + E_{\text{scr}} \quad (\text{S1})$$

where $E_{P,\text{BTO}}$ and $E_{P,\text{SNO}}$ are the energy per unit area of polarizing a slab of thickness d_{BTO} and d_{SNO} , respectively, E_{d} is the energy cost of the depolarizing field and E_{scr} the energy required to form screening charges by electron-hole excitation across the band gap [34, 35]. The energy contribution needed to form polar displacements P is described by

$$E_{P,\text{ABO}} = aP_{\text{ABO}}^2 + bP_{\text{ABO}}^4 \quad (\text{S2})$$

and we obtain a and b from fitting the curve to the energy profile obtained from modulating bulk BaTiO₃ and SmNiO₃ according to their lowest polar phonon mode. The calculated energy profiles are shown as the symbols in Fig. S3 and the a and b parameters of the fits (solid lines in Fig. S3) are given in Tab. I.

In contrast to Refs. [34] and [35], we have an interface to a conducting material. For an imperfect metal, the depolarizing field ε_d depends on the finite screening length λ following

$$\varepsilon_d \simeq -\frac{2\lambda\sigma_{\text{inter}}}{\epsilon_0\epsilon_r d_{\text{BTO}}} \quad (\text{S3})$$

where λ is the finite screening length, ϵ_0 is the dielectric constant in vacuum, ϵ_r is the relative permittivity of BaTiO₃, σ_{inter} is the interface charge from the different polarization contributions and d_{BTO} the ferroelectric film thickness [36]. This equation is valid for the case of $d_{\text{SNO}} \gg d_{\text{BTO}} \gg \lambda$ and short-circuit boundary conditions. Note that in the insulating case, the depolarizing field is given by [34, 35]

$$\varepsilon_d = -\frac{\sigma_{\text{inter}}}{\epsilon_0\epsilon_r} \quad (\text{S4})$$

and we recover this field from Eq. S3 when $\gamma = \frac{2\lambda}{d_{\text{BTO}}} = 1$. Simulating a metal-to-insulator transition in this model would correspond to varying γ from close to zero to a value of 1.

We obtain the electrostatic energy cost associated with the depolarizing field by integrating over the BaTiO₃ slab according to

$$E_d = \frac{\epsilon_0\epsilon_r}{2}\varepsilon_d^2 d_{\text{BTO}} = \frac{2}{\epsilon_0\epsilon_r}\lambda^2\sigma_{\text{inter}}^2 \frac{1}{d_{\text{BTO}}} = \frac{1}{2\epsilon_0\epsilon_r}\gamma^2\sigma_{\text{inter}}^2 d_{\text{BTO}}. \quad (\text{S5})$$

We also include an additional screening cost for carriers generated by electron-hole excitation across the band gap E_g [34, 35]. This screening energy is given by

$$E_{\text{scr}} = \frac{\sigma_{\text{scr}}}{e} E_g \quad (\text{S6})$$

where e is the electronic charge and σ_{scr} are the additional carriers.

We determine if σ_{scr} is non-zero by finding the minimum of the total electrostatic energy according to

$$\frac{\partial E_{\text{es}}}{\partial \sigma_{\text{scr}}} = 0 \quad (\text{S7})$$

Solving this equation for σ_{scr} we obtain the following condition

$$\sigma_{\text{scr}} = \begin{cases} 0 & \text{if } d_{\text{BTO}} \leq \frac{\epsilon_0\epsilon_r}{\gamma^2} \frac{E_g}{e} \frac{1}{P_{\text{tot}}} \\ P_{\text{tot}} - \frac{\epsilon_r\epsilon_0}{\gamma^2} \frac{E_g}{e} \frac{1}{d_{\text{BTO}}} & \text{if } d_{\text{BTO}} > \frac{\epsilon_0\epsilon_r}{\gamma^2} \frac{E_g}{e} \frac{1}{P_{\text{tot}}} \end{cases} \quad (\text{S8})$$

with $P_{\text{tot}} = P_{\text{layer}} - P_{\text{BTO}} + P_{\text{SNO}}$.

This leads to a total $\sigma_{\text{inter}} = P_{\text{layer}} - P_{\text{BTO}} + P_{\text{SNO}} - \sigma_{\text{scr}}$. We obtain the polarization that minimizes the total energy by calculating the energy landscape for a range of polarization values and determining the global minimum. To model the unhappy orientation, we restrict the polarization of BaTiO₃ to values of less than zero.

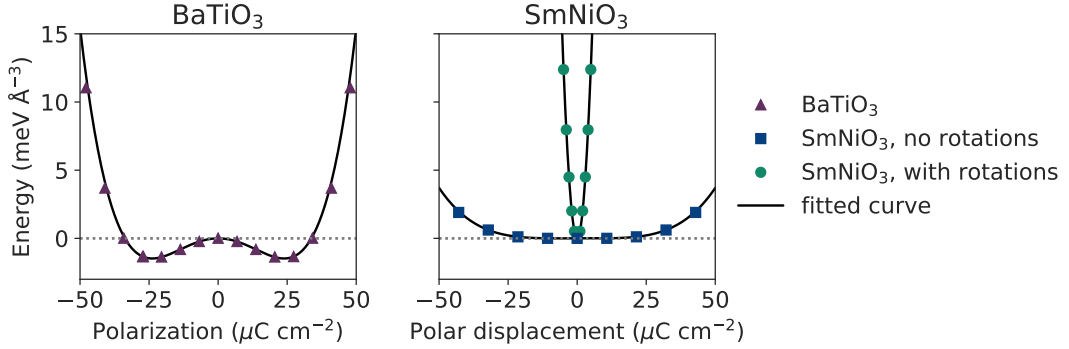


Figure S3: Calculated energy as a function of polarization as obtained from freezing in the lowest polar phonon mode for bulk BaTiO₃ (left) and bulk SmNiO₃ with active (circles) and disabled (squares) rotations (right). The curve obtained from fitting Eq. S2 is shown in black.

parameter	BaTiO ₃		SmNiO ₃	
	rotations	no rotations	rotations	no rotations
a (eV m ⁴ C ⁻²)	-3.243	1090.189	-0.020	
b (eV m ⁸ C ⁻⁴)	28.464	-6121.441	3.348	

Table I: Parameters obtained from fitting Eq. S2 to the DFT energies calculated as a function of the lowest polar phonon mode as shown in Fig. S3.

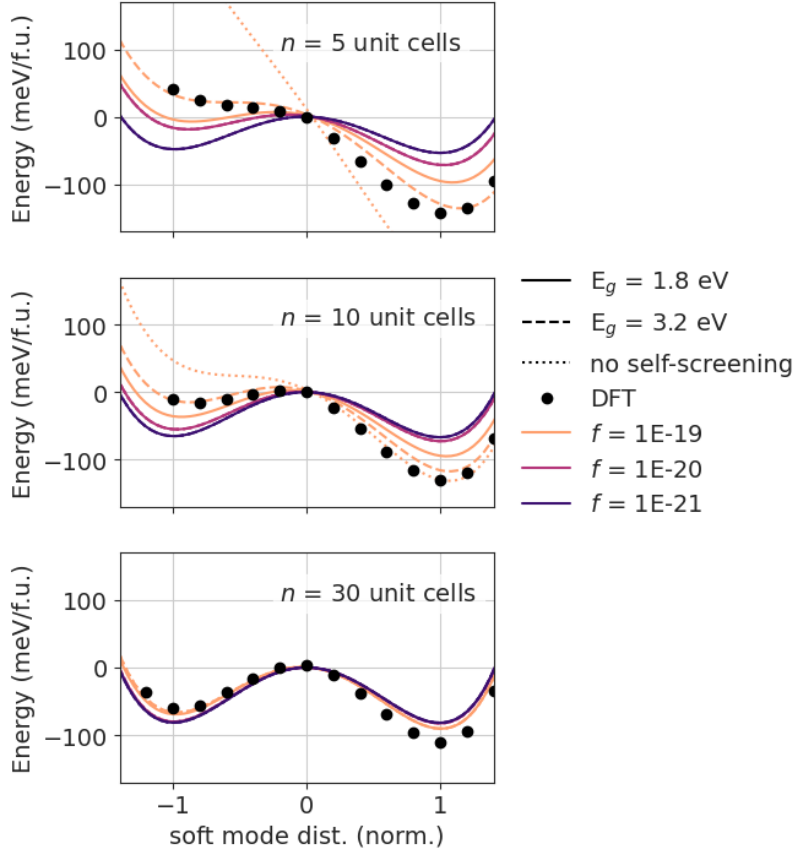


Figure S4: Comparison of DFT results to the electrostatic model with different factors $\frac{\lambda^2}{\epsilon_r}$ and electronic band gaps $E_g = 1.8$ eV (full line), 3.2 eV (dashed line) or no excitations across the band gap (dotted line). We show the energy divided by the total number of formula units in the superlattice as a function of the soft mode distortion of BaTiO_3 where -1 corresponds to the ‘unhappy’ and 1 to the ‘happy’ orientation and for $(\text{BaTiO}_3)_n(\text{SmNiO}_3)_4$ superlattices with $n = 5, 10$ or 30 unit cells.

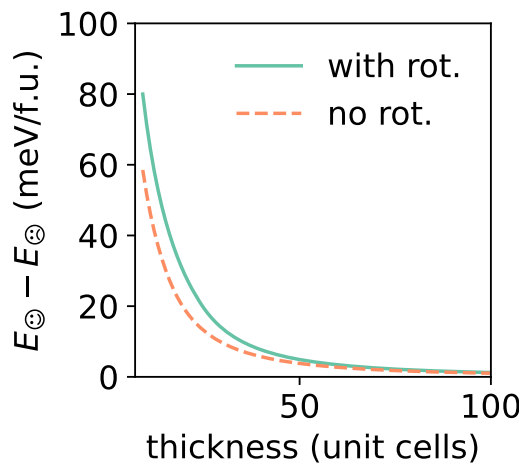


Figure S5: DFT energy differences between happy and unhappy superlattices with active (green solid) and disabled (blue dashed) rotations for slab thicknesses from 8 to 100 BaTiO_3 and SmNiO_3 unit cells.